Random walks on random Koch curves

Random walks on random Koch curves

S Seeger[1], K H Hoffmann[1] and C Essex[2]

[1] Institut für Physik, Technische Universität, D-09107 Chemnitz, Germany
[2] Department of Applied Mathematics, The University of Western Ontario, London, ON N6A
5B7, Canada

Abstract
Diffusion processes in porous materials are often modeled as random walks on
fractals. In order to capture the randomness of the materials random fractals
are employed, which no longer show the deterministic self-similarity of regular
fractals. Finding a continuum differential equation describing the diffusion on
such fractals has been a long-standing goal, and we address the question of
whether the concepts developed for regular fractals are still applicable. We
use the random Koch curve as a convenient example as it provides certain
technical advantages by its separation of time and space features. While
some of the concepts developed for regular fractals can be used unaltered,
others have to be modified. Based on the concept of fibers, we introduce
ensemble-averaged density functions which produce a differentiable estimate
of probability explicitly and compare it to random walk data.

PACS numbers: 05.45.Df, 66.10.Cb, 05.40.Fb

(Some figures in this article are in colour only in the electronic version)

1. Introduction

The diffusion of hydrogen in amorphous metals [1] and diffusion of water in biological tissues
[2] are two examples where anomalous diffusion is observed. Such diffusion processes have
been successfully modeled using random walks on fractal structures [3]. These processes are
characterized microscopically by a time-dependent distribution of particles $P(r, t)$, where the
mean square distance $\langle r^2(t) \rangle$ a particle has moved in time t from its starting point relates to t
by a power law

$$\langle r^2(t) \rangle \propto t^{2/d_w}, \tag{1}$$

with $d_w \geqslant 2$ denoting the random walk dimension of the underlying fractal structure.

In the literature, many suggestions [4–10] have been given to generalize or develop from
the well-known Euclidean diffusion equation

$$\frac{\partial P(x, t)}{\partial t} = D \frac{\partial^2 P(x, t)}{\partial x^2}, \tag{2}$$

where D denotes the diffusion constant, to the case of anomalous diffusion. All these approaches were at best partially successful [11, 12] because there is no physical theory for generalizing diffusion equations in terms of the underlying fractal dynamics. As a result, random walks on them are not naturally described by differential or integral equations. In [11], we explained that the common way to treat this problem is to look at some type of averaged quantity. But even the angle-averaged probability, $P(r, t)$, remains a fractal itself, not amenable to such treatment [4, 5, 11].

Previously [11, 13] we proposed an alternative approach, which left behind heuristic differential equations to work with fractals directly instead. We used the natural similarity group in connection with the random walk on the fractal to study probability distributions and the observation that probability densities on the fractal—like the generalized diffusion equations cited in [10, 11]—are invariant under a one-parameter group. This allows one to introduce a similarity variable η as a proper rescaling of r and then to separate the probability density as a product of one function depending on time t only and another function G depending on η only.

In [14], we applied this approach to the Sierpinski gasket and plotted $G(\eta)$. This led to a family of smooth functions that might be described as a 'multivalued' function, plotted against the similarity variable η all in one graph. The resulting, multivalued $G(\eta)$ appears like a muscle-shaped family of well-defined differentiable curves which we called fibers. These reveal a fully differentiable structure, intrinsic to the random walk behavior, which is not apparent in the Euclidean space.

However, direct analysis of the Sierpinski muscle is not straightforward. The family of fibers have subtle wavelike behavior, which presumably have to do with the inherent multiple connectedness of the fractal. If that is so, a simpler fractal, the Koch curve, should not have them. This was established in [13]. Unlike the fibers for the Sierpinski gasket, the fibers of the Koch curve indeed do not oscillate or cross one another.

The Koch curve's one-dimensional generator ensured that probability at any iteration depth is easily defined as a function of a single space parameter, ℓ, the chemical distance. All the dynamical information about the random walk on the Koch curve is given by combining the analysis of its fibers and the probability density $P(\ell, t)$. This allows the reconstruction of $P(\mathbf{r}(\ell), t)$ directly from the fibers. This reconstruction successfully matched the corresponding values computed from a master equation. All fibers belong to a one-parameter family, which we found could be fully represented by a single first-order differential equation in η.

How could the Koch muscle give insight into the Sierpinski gasket's muscle? Clearly, multiple connectedness needs to be understood. One way to introduce that into this approach with a single fractal curve is by folding the curve back onto itself. This suggests that there are two different aspects to multiple connectedness. While there is the obvious back flow of probability from new directions, there is also something basic to consider first. Unlike the Koch case, in the case of multiple connectedness one can have more than one ℓ for a given $\mathbf{r}$. How does this affect the muscle?

How can we generate such curves? Random fractals [15–17] suggest one approach. Random fractals arise in connection with processes such as diffusion-limited aggregation or in representing realistic natural structures through iterated function systems or stochastic point sets generated from probability measures [18]. However, the approach we consider is to expand the complexity of the Koch analysis incrementally so as not to compromise understanding. As long as the one dimensionality of the generator is preserved for the random curves, many of the original characteristics of the analysis will be preserved too.

Random Koch curves introduce new issues. Individual realizations of the curves are not strictly self-similar. Responding to this leads naturally to the treatment of the ensemble of
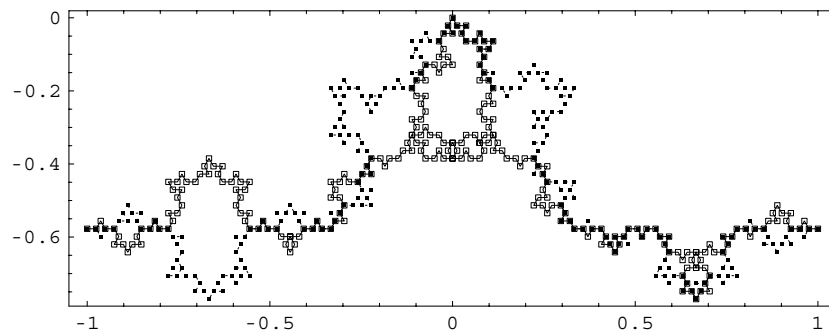
Figure 1. Two different realizations of random Koch curves of depth 4 with *L* and *R* generators chosen with equal probability. Due to the irregular choice of the left or right refinement, the curve may fold back onto itself.

random Koch curves, which puts a different framework on the muscle approach. We begin by defining a class of random Koch curves and exploring their basic properties. Then we examine diffusion processes on this class of curves, applying the idea of fibers and muscles as in [11, 13].

2. Random Koch curves

To construct a Koch curve [19], we begin with an oriented straight line segment starting at $\mathbf{r}_l = (-1, -1/\sqrt{3})$ and terminating at $\mathbf{r}_r = (1, -1/\sqrt{3})$ as in [13], which we also refer to as a Koch curve of iteration depth 0. The Koch curve of iteration depth 1, also referred to as the generator of the Koch curve, is constructed by dividing the line into three equal segments, adding an equilateral triangle with the middle segment as its base and removing the middle segment. The orientation of the remaining segments follows the orientation of the one side removed. Thus a Koch curve generator has four equal segments, each joined head to tail, with the start and end points oriented as in the original line. As the triangle may point to the left (*L*) or right (*R*) of the original line, there are two possible generators.

For the regular curve, either the left or the right generator is selected in all subsequent refinements. But what if we choose the generator refinement of each segment according to some external rule or at random? For instance, we might choose generator *R* with some probability $p_R = q$ and generator *L* with probability $p_L = 1 - q$. In the following a generic random Koch curve of iteration depth *M* is denoted by $\mathcal{C}^M$, where the index *M* is not used if unnecessary. Figure 1 shows two different realizations, $\mathcal{C}_1^4$ and $\mathcal{C}_2^4$, of random Koch curves of depth 4 resulting from a refinement with $q = \frac{1}{2}$.

As can be seen from the figure, the self-similarity of a fractal is present only in a statistical manner. Further, the curves can develop loops in the sense that the random curve may fold back onto itself. This allows more complicated random walker paths, which can mimic some aspects of the lacunae of the Sierpinski gasket. However, the equivalence to the lacunae of Sierpinski gaskets is not complete, as we treat the paths as *not* connected at crossings in this paper.

Ω^M is the ensemble of random Koch curves of depth *M*. $|\Omega^M|$ is the total number of distinct realizations of depth *M* possible: $|\Omega^M| = 2^{\frac{4^M-1}{4-1}}$. This is because a curve of depth *M* has 4^M segments. Thus for each curve $\mathcal{C}^{(M-1)} \in \Omega^{(M-1)}$, there are $4^{(M-1)} R/L$-choices to
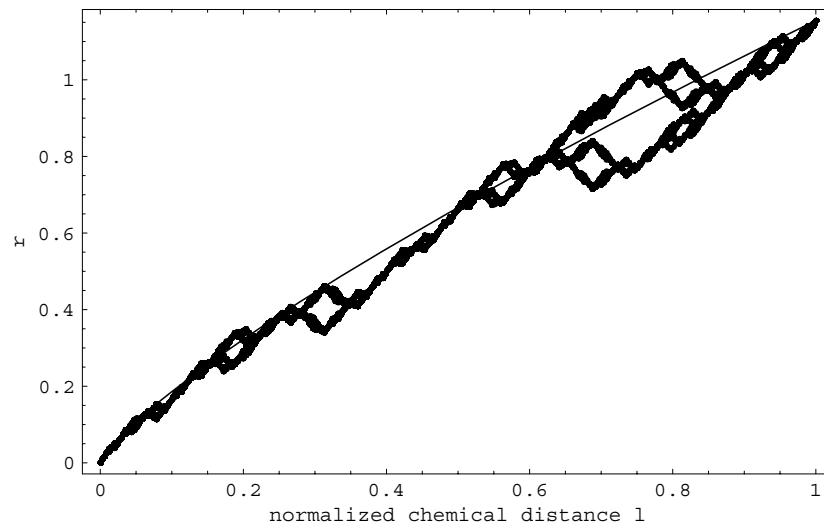
Figure 2. Euclidean distance *r* versus normalized chemical distance ℓ, both measured with respect to $\mathbf{r}_0$, for 20 realizations of random Koch curves of iteration depth 4 with generators chosen with equal probability.

generate all the curves of depth *M* from a given $\mathcal{C}^{(M-1)}$. Initially, there are $2 = 2^{(4^0)}$ curves of depth 1. Then by iteration, we find $|\Omega^M| = 2^{\sum_{m=0}^{M-1} 4^m}$.

3. Random walks on Koch curves

In order to discuss random walk processes on Koch curves, we introduce the *unitless chemical distance* $\lambda_{(M)}$ as the number of segments between $\mathbf{r}_0$ and the point in question. Points which lie between $\mathbf{r}_0$ and $\mathbf{r}_r$ have positive $\lambda_{(M)}$ and points which lie between $\mathbf{r}_0$ and $\mathbf{r}_l$ have negative $\lambda_{(M)}$. Also, we introduce the *normalized chemical distance*

$$\ell = \frac{\lambda_{(M)}}{2 \cdot 4^{(M-1)}}. \tag{3}$$

Note that with this choice made, ℓ becomes independent of the iteration depth. The magnitude of $\mathbf{r}$, $r(\ell)$, is the Euclidean distance from the origin.

Figure 2 shows an ensemble of typical $r(\ell)$-relations for 20 realizations of random Koch curves. It is apparent that in the ensemble, there are points with the same normalized chemical distance ℓ but different Euclidean distance *r*. An interesting feature is the occurrence of eye patterns in figure 2. In contrast to the loops in figure 1, which are due to the orientation of the generators at higher levels, these eye patterns in figure 2 are due to the overlay of data from different realizations of the random Koch curve. The most striking feature is the self-similarity of the graph, which can be traced directly back to the structure of the random generation scheme.

In the following, we use the scaling exponents introduced in [13]. For the normalized chemical distance we find $\ell = \alpha r^{d_f}$, with some constant α. This relation is reflected in the analogous change of variables for a differential equation in [10]. The proportionality constant, α, plays a key role for the explicit fractal, especially so for the random case.
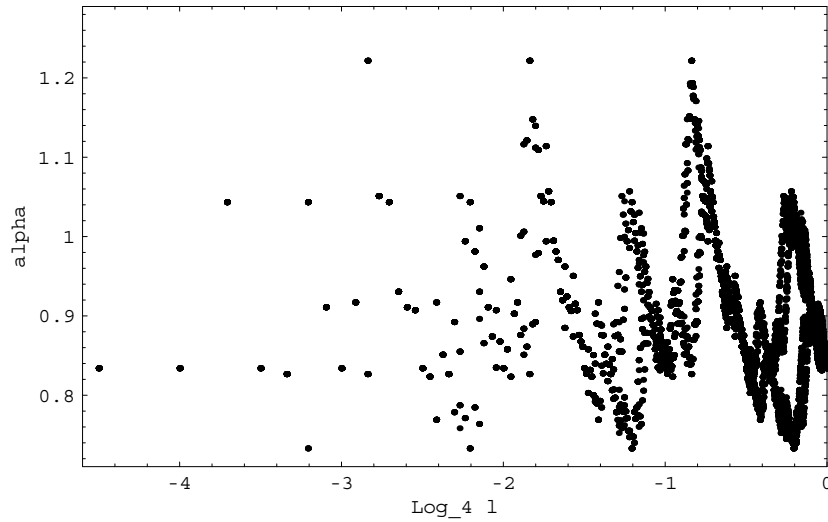
Figure 3. For 20 realizations of a random Koch curve of iteration depth 4, the α values are shown as a function of the normalized chemical distance. Note that the structure present in figure 5 of [13] reappears here in addition to α-values lying outside the range of the regular Koch curve. This is expected because the regular Koch curve is a realization of the ensemble.

The normalized chemical distance ℓ serves as the natural independent parameter

$$\alpha(\ell) = \frac{\ell}{r(\ell)^{d_f}}, \tag{4}$$

which means that there is only one value of α for each ℓ. As there are 4^M segments at depth M, we may determine $\alpha(i)$ for the endpoint of each segment and form the tuple $\gamma_{\mathcal{C}^M} = (\alpha(1), \alpha(2), \ldots, \alpha(4^M))$ for any realization $\mathcal{C}^M$.

Figure 3 shows α obtained from (4) for 20 different realizations of a random Koch curve of iteration depth 4. It shows that α are still confined to a limited domain, which is larger than that for the regular Koch curve (see figure 5 of [13]).

4. Ensemble properties of random Koch curves

While the individual realizations of the Koch curve are randomly selected, the union of the points on all random Koch curves is fully determined. Figure 4 shows 20 realizations to iteration depth 4 which are overlaid on the same plot. The lines join individual points in each realization. Even though there are more than 10^{25} possible realizations at iteration depth 4, the appearance of the union of the whole ensemble is clearly depicted with only 20 realizations, indicating considerable redundancy in individual elements of the realizations. The set can also be produced by a generator where the middle segment of the line is replaced by a diamond rather than a triangle. The set of all α can thus be determined in principle for the entire ensemble at any iteration depth.

For the regular Koch curve, the extreme values of α at any iteration depth converge with increasing iteration depths. We find $\alpha_{\min}^{\text{reg}} = 17 \times 2^{1-d_f} \times 91^{-d_f/2} = 0.823387\ldots$ and $\alpha_{\max}^{\text{reg}} = 47 \times 2^{1-d_f} \times 307^{-d_f/2} = 1.05697\ldots$. Surprisingly, the $\alpha_{\min}$ value is already obtained for iteration depth $M = 3$, while the $\alpha_{\max}$ value is obtained for iteration depth
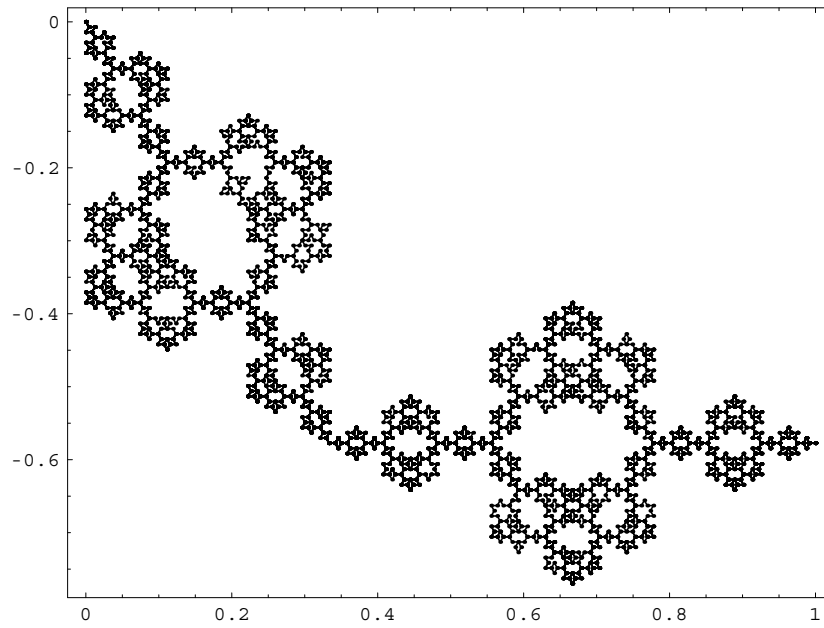
Figure 4. An overlay of 20 random Koch curves of iteration depth 4. Note that already this small number gives a good idea of the ensemble of all possible random Koch curves.

$M = 4$. The corresponding echo-point classes include $\mathbf{r}_{min}^{reg} = (11/27, -1/\sqrt{3})$ and $\mathbf{r}_{max}^{reg} = (17/27, -19/(27 \cdot \sqrt{3}))$, respectively. For the random Koch curve α_{min}^{ran} and α_{max}^{ran} might be expected to fluctuate, depending on the realizations considered. In order to find the extreme values possible, we created the respective extreme realizations by orienting the inserted triangles such that their tip was always positioned as far or as close as possible to the origin. The result was $\alpha_{min}^{ran} = 3 \times 2^{1-d_f} \times 7^{-d_f/2} = 0.732987\ldots$ and $\alpha_{max}^{ran} = 5 \times 2^{1-d_f} \times 7^{-d_f/2} = 1.22164\ldots$.

5. Dynamics on random Koch curves

In order to describe random walks on the Koch curve, we note that the topology of regular and random Koch curves is that of a line, given that coincident points are considered distinct. Thus, the reasoning can proceed similar to that in [13]. The probability density function for the walk is given by

$$P(\ell, t) = t^{-1/2} G_\alpha(\eta) \qquad \text{with} \qquad G_\alpha(\eta) = \frac{1}{2\sqrt{D\pi}} \exp\left(-\frac{\alpha^2}{4D}\eta^{d_w}\right). \qquad (5)$$

As before, points of the curve are treated according to their respective values of α. This approach again leads to the fibers associated with the echo-point classes and to a cloud of such fibers for the whole fractal, which was termed muscle. As equation (5) just depends on α, and no longer on the distinct values of r or l, each member of an echo-point class produces the same fiber $G_\alpha(\eta)$, which is the general solution of the same differential equation we deduced in [13]. The only way that $G_\alpha(\eta)$ can differ from the result of [13] is for the range of α values to be different.
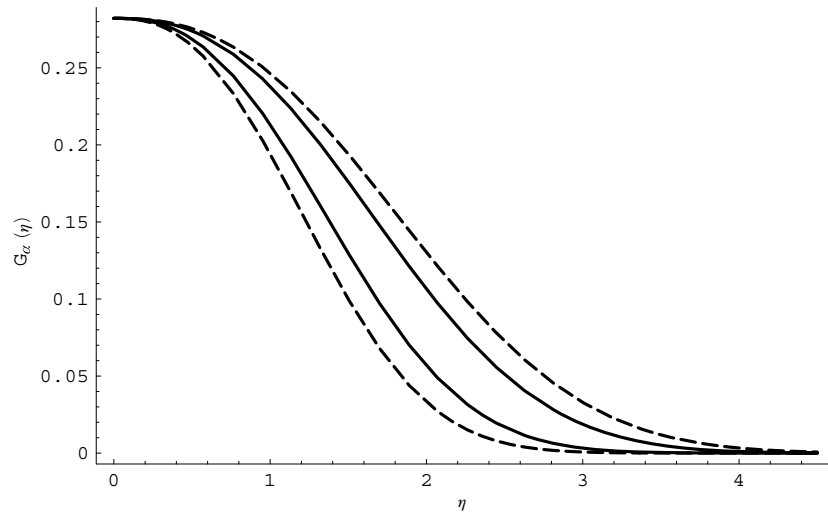
Figure 5. The muscle created by the α values for random Koch curves are shown. The resulting muscle shape is bounded by the fibers for $\alpha = \alpha_{min}^{ran}$ and $\alpha = \alpha_{max}^{ran}$ depicted by dashed lines. For comparison, the outline of the muscle for a regular Koch curve is shown by its bounding fibers depicted by solid lines.

As α has an upper and a lower bound, a plot of $G_\alpha(\eta)$ for different echo-point classes α looks like a muscle too, where the top and bottom fibers are given by α_{min} and α_{max}, respectively. For any given realization the different echo-point classes will have different sizes; none the less, all points in one class with the same α will produce one single fiber. Figure 5 shows the envelopes of the muscle shape $G_\alpha(\eta)$ created by the possible α values produced by an ensemble of random Koch curves. The boundaries of the muscle are given by $G_\alpha(\eta)$ for $\alpha = \alpha_{min}^{ran}$ and $\alpha = \alpha_{max}^{ran}$ respectively. Clearly, the muscle is larger than that of the regular Koch curve itself.

6. Ensemble and realization-averaged *G*-density functions

For random Koch curves, a good option is to work with quantities averaged over the ensemble of random Koch curves. This produces explicitly what the heuristic differential equations were meant to produce: a differentiable averaged probability density function on the fractal.

What would a simple explicit averaging strategy be for a representative probability for any particular point, at some time? One way would be to multiply the appropriate prefactor by an ensemble average of $G(\eta)$ for iteration depth M:

$$\langle G^{(M)}\rangle(\eta) = \frac{1}{N_e} \sum_{\alpha \in \Gamma^M} G_\alpha(\eta), \tag{6}$$

where Γ^M is the concatenation of γ_{C^M} of the full ensemble Ω^M and N_e is the number of elements in Γ^M. However, with Ω^M so large, even computing this ensemble directly is problematic. But an alternative strategy is possible by successively building up a list of all possible α values for a given ℓ, while at the same time keeping track of the fraction w_ℓ of realizations of random Koch curves in which these values occur. The method is based on the fact that in constructing a random Koch curve in each iteration step, an L or R decision has to be taken. An overlay of both decisions will give a diamond replacing the middle section of a
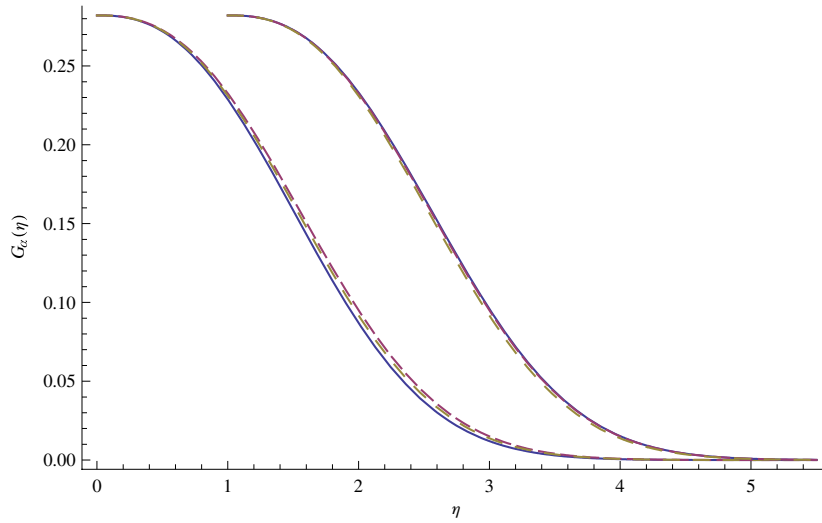
Figure 6. A comparison between the realization-averaged *G*-density function of iteration depth 5 and of iteration depth 7 for a single realization of a random Koch curve to the ensemble-averaged *G*-density function of iteration depths 1 (long dash) and 2 (short dash). Note that already the ensemble-averaged *G*-density function of iteration depth 1 provides a very reasonable approximation. The data for iteration depth 7 were shifted one unit to the right for better readability.

segment. In this way, all possible points of all possible realizations of a random Koch curve are generated. Figure 4 shows this: the figure—up to few missing points—could as well be generated by using a diamond generator instead of the *L* or *R* generator and then building up the overlay. Thus, $\langle G^{(M)}\rangle(\eta)$ can be written as

$$\langle G^{(M)}\rangle(\eta) = \frac{1}{N_e} \sum_{\alpha \in \Gamma^M} G_\alpha(\eta) = \sum_\ell \sum_{\alpha(\ell)} w_{\ell,\alpha(\ell)} G_{\alpha(\ell)}(\eta). \tag{7}$$

We note as an interesting side issue that echo points, i.e. points which echo each other in the sense that their **r** and ℓ values are obtained by multiplication with 3 and 4 respectively, have the same $w_{\ell,\alpha(\ell)}$.

We now introduce the *realization average*, which is the corresponding averaged *G*-density function of iteration depth *M* for a single realization:

$$\bar{G}^{(M)}(\eta) = \frac{1}{N_c} \sum_{\alpha \in \gamma_{\mathcal{C}^M}} G_\alpha^{(M)}(\eta), \tag{8}$$

where N_c is the number of elements in $\gamma_{\mathcal{C}^M}$. $\bar{G}^{(M)}(\eta)$ is motivated as above, but for a particular realization only.

It is interesting to compare $\bar{G}^{(N)}(\eta)$ to $\langle G^{(M)}\rangle(\eta)$ for the case where $N > M$. In figure 6 we considered $N = 5$ and $M = 1, 2$ and $N = 7$ and $M = 1, 2$. The comparison shows that the ensemble-averaged *G* of iteration depth 2 (short dash) agrees very well with the realization-averaged *G* of iteration depth 5. And even the ensemble-averaged *G* of iteration depth 1 (long dash) provides a reasonable approximation to the data from a single realization. The comparison with the realization-averaged *G* of iteration depth 7 shows similar behavior. We analyzed other iteration depths and again found the same behavior.

The surprising similarity of these curves, despite different realizations and different iteration depths, arises because a random Koch curve of high enough iteration depth contains
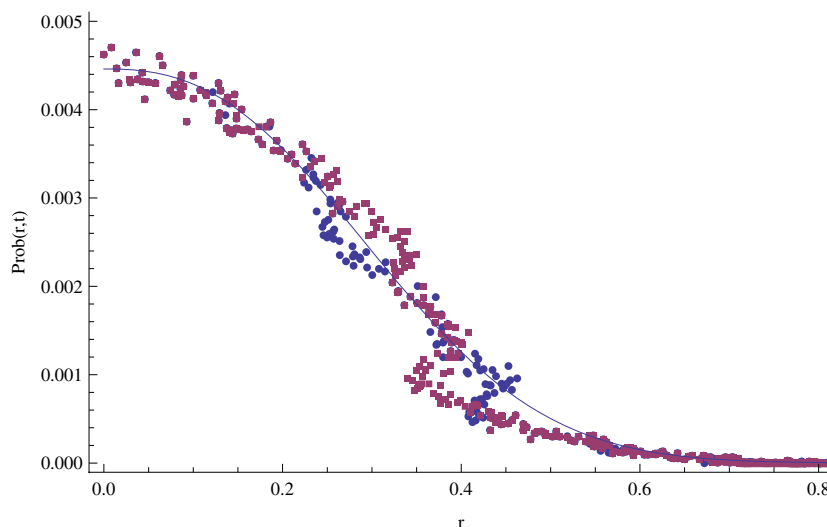
Figure 7. The probability $P(r, t_0 = 10\,000)$. The data points (circles and squares) are determined from an ensemble of 200 000 random walkers walking on two random Koch curves of iteration depth 4 with transition probability $w = 0.4$. The solid curve is produced based on (5) by using the ensemble-averaged G-density function $\langle G^{(2)} \rangle$.

a good representation of the alpha spectrum of the full ensemble. The full ensemble produces a fractal in its own right, which can be produced independently by the diamond generator. The possible alpha values are thus limited by that fractal, making it easier to approximate the whole with any sample. If some members of an echo class are missing because the curve has folded in a way excluding them, only one member is necessary to generate a fiber.

Any of these averages with a suitable pre-factor will be a fairly robust smooth representation of probability on the fractal. This estimate will not directly reflect the fractal-like or specific stochastic nature of any one of these objects because of the averaging procedures. This will also be true of the solutions of all heuristic differential equations. However, in our case the nature of the average is explicit.

To demonstrate the applicability of these results, we use (5) for a comparison with the probability $P(r, t_0)$ of walkers on a random Koch curve of iteration depth 4, which started at the origin at time $t = 0$. The transition probability for a random walker to move one step backward or forward was chosen as $w = 0.4$ and $t_0 = 10\,000$; for details, see [13]. Therefore, we can compare the probability from the random walks with the approximation based on (5). In figure 7, we show the random walk data for two different random Koch curves. The line depicts $P(r, t_0)$ based on $\langle G^{(2)} \rangle$. Note that $P(r, t_0)$ is the probability of finding a random walker at a point on the random Koch curve, which is at distance r from the origin. The results show that the approximation works quite well, even though one sees very well the deviations of the random walk data due to the fractal nature of the Koch curve ensemble.

7. Conclusion

In this paper, we considered the problem of a random walker moving on a random Koch curve. In a regular Koch curve, the chemical distance corresponds to a unique Euclidean distance, but this is not necessary in the random case. The curve may fold back onto itself, permitting points to fall onto each other. This is the first step in considering multiple connectedness for fractals

such as the Sierpinski gasket. If we presume that concurrent points remain separate entities, the curve remains one dimensional. This approach allows previous work to be applied directly to random walks on random Koch curves: the time development can be completely separated from the structural features of the fractal on which the walks take place. The transition to the random Koch curve surprisingly only expands the previously discovered muscle for the regular Koch curve. It does not alter it qualitatively. As a result, the original differential equation for the fiber family continues to hold for the entire ensemble of random curves.

The corresponding ensemble of fibers implies a natural average to produce a direct differentiable average probability. We directly apply the similarity group approach and deal with the multivalued *G*-density. The resulting fibers are calculated explicitly using the separation of time and space features.

For random Koch curves, the new concept of ensemble and realization-averaged *G*-density functions is introduced. The self-similarity present in the random Koch curve is nicely caught in the realization-averaged *G*-density functions studied. This quantity shows a strong self-averaging tendency, which explains the similarity with the ensemble-averaged *G*-density functions of low iteration depth and with the random walk data.

The results obtained can be easily generalized to any fractal that is topologically equivalent to a straight line. The generalization to more complicated, especially lacunar, fractals is the next step. The concept of fibers, clouds and echo points which was introduced in [14] for the example of the Sierpinski gasket has proven its versatility also in the case of a random fractal.

References

[1] Schirmacher W, Perm M, Suck J-B and Heidemann A 1990 Anomalous diffusion of hydrogen in amorphous metals *Europhys. Lett.* **13** 523–9
[2] Köpf M, Corinth C, Haferkamp O and Nonnenmacher T F 1996 Anomalous diffusion of water in biological tissues *Biophys. J.* **70** 2950–8
[3] Havlin S and Ben-Avraham D 1987 Diffusion in disordered media *Adv. Phys.* **36** 695–798
[4] O'Shaughnessy B and Procaccia I 1985 Analytical solutions for diffusion on fractal objects *Phys. Rev. Lett.* **54** 455–8
[5] O'Shaughnessy B and Procaccia I 1985 Diffusion on fractals *Phys. Rev.* A **32** 3073–3083
[6] Giona M and Roman H E 1992 Fractional diffusion equation for transport phenomena in random media *Physica* A **185** 87–97
[7] Giona M and Roman H E 1992 Fractional diffusion equation on fractals: one-dimensional case and asymptotic behaviour *J. Phys. A: Math. Gen.* **25** 2093–105
[8] Metzler R, Glöckle W G and Nonnenmacher T F 1994 Fractional model equation for anomalous diffusion *Physica* A **211** 13–24
[9] Compte A and Jou D 1996 Non-equilibrium thermodynamics and anomalous diffusion *J. Phys. A: Math. Gen.* **29** 4321–9
[10] Campos D, Méndez V and Fort J 2004 Description of diffusion and propagative behavior on fractals *Phys. Rev.* E **69** 031115/1–031115/5
[11] Schulzky C, Essex C, Davison M, Franz A and Hoffmann K H 2000 The similarity group and anomalous diffusion equations *J. Phys. A: Math. Gen.* **33** 5501–11
[12] Fischer A, Seeger S, Hoffmann K H, Essex C and Davison M 2007 Modeling anomalous superdiffusion *J. Phys. A: Math. Theor.* **40** 11441–52
[13] Essex C, Davison M, Schulzky C, Franz A and Hoffmann K H 2001 The differential equation describing random walks on the Koch curve *J. Phys. A: Math. Gen.* **34** 8397–406
[14] Davison M, Essex C, Schulzky C, Franz A and Hoffmann K H 2001 Clouds, fibres and echoes: a new approach to studying random walks on fractals *J. Phys. A: Math. Gen.* **34** L289–96
[15] Franz A, Schulzky C, Do Hoang N A, Seeger S, Balg J and Hoffmann K H 2006 Random walks on fractals *Parallel Algorithms and Cluster Computing* ed K H Hoffmann and A Meyer (Berlin: Springer) p 303
[16] Do Hoang N A, Hoffmann K H, Seeger S and Tarafdar S 2005 Diffusion in disordered fractals *Europhys. Lett.* **70** 109–15

[17] Do Hoang N A, Blaudeck P, Hoffmann K H, Prehl J and Tarafdar S 2007 Anomalous diffusion on random fractal composites *J. Phys. A: Math. Theor.* **40** 11453–65

[18] Barnsley M, Hutchinson J and Stenflo Ö 2005 A fractal valued random iteration algorithm and fractal hierarchy *Fractals* **13** 111–46

[19] von Koch H 1904 Sur une courbe continue sans tangente obtenue par une construction géométrique élémentaire *Arkiv för Matematik, Astronomi och Fysik* **1** 681–704